

**Cu-Au type orderings in the staggered quadrupolar region of the  
fcc Blume Emery Griffiths model**

A. Özkan<sup>1</sup>, B. Kutlu<sup>2</sup>

<sup>1</sup>Gazi Üniversitesi, Fen Bilimleri Enstitüsü, Fizik Anabilim Dalı, Ankara,  
Turkey

<sup>2</sup>Gazi Üniversitesi, Fen -Edebiyat Fakültesi, Fizik Bölümü, 06500  
Teknikokullar, Ankara, Turkey

E-mail: aycan@gazi.edu.tr and bkutlu@gazi.edu.tr

The spin-1 Ising (BEG) model has been simulated using a cellular automaton (CA) algorithm improved from the creutz cellular automaton (CCA) for a face-centered cubic (fcc) lattice. The simulations have been made in the staggered quadrupolar region for  $-24 \leq d = D/J < 0$  and  $-3 \leq k = K/J \leq -1.35$  parameter region. The ground state diagram ( $k, d$ ) of the fcc BEG model has ferromagnetic (F), quadrupolar (Q) and staggered quadrupolar (SQ) ordering regions. The staggered quadrupolar ordering region separates into three ordering regions ( $A_3B$ ,  $AB$  and  $AB_3$ ) which have the different stoichiometric Cu-Au type structures. The phase diagrams on the  $(kT_C/zJ, d)$  plane for  $k = -3$  and on the  $(kT_C/zJ, k)$  plane for  $d = -4$  including three ordering regions are obtained and compared with the results of the other methods.

Key words: Phase transitions and critical phenomena, Phase diagrams (Theory), Cellular automaton

## 1 . Introduction

The Blume-Emery-Griffiths (BEG) model is a spin-1 Ising model with

very rich and interesting phase structure. The BEG model was firstly studied to determine the phase separation and superfluid ordering in He<sup>3</sup>-He<sup>4</sup> mixtures [1]. The versions and extensions of the model have applied to the solid-liquid-gas systems [2], the multicomponent fluids [3], the microemulsions [4], the semiconductor alloys [5], the binary alloys [6] and the reentrant phenomenon in the phase diagrams [7] – [9].

The BEG model is defined by the following Hamiltonian:

$$H_I = -J \sum_{\langle ij \rangle} S_i S_j - K \sum_{\langle ij \rangle} S_i^2 S_j^2 + D \sum_i S_i^2 \quad (1)$$

where  $s_i = -1, 0, 1$  and  $\langle ij \rangle$  denotes summation over all nearest-neighbor (nn) pairs of sites. The parameters  $J$ ,  $K$  and  $D$  are bilinear, biquadratic interaction terms and the single-ion anisotropy constant. The BEG model has been investigated by different techniques. For  $k \geq 0$  the model has been studied using the mean-field approximation (MFA) [1, 2], the cellular automaton [8, 9], the series expansion method [10], the transfer matrix method [11], the position space renormalization method [12], the constant coupling approximation [13], the linear chain approximation [14], the cluster variation method (CVM) [15], the monte carlo method (MC) [16], the probabilistic limit theorem [17] and the cellular automaton (CA) [8, 9], [18 – 23]. However, the phase diagrams of the model for  $k < 0$  have been studied by MFA [7], the renormalization group theory (RG) [24, 25], the MC [26] – [30], the Bethe approximation [29], the CVM [30] – [34], the monte carlo renormalization group (MCRG) [35] and the two-particle cluster approximation (TPCA) [36] on the different lattice type and the phase boundary. The special orders

of the Cu-Au ( $A_3B$ ,  $AB$  and  $AB_3$ ) type binary alloys are investigated by the MC [37] [41], the CVM [42, 43] and the mean field theory [44, 45] considering also the spin-1/2 Ising model, the effective medium theory [40, 45] (EMT) and the Bozzola Ferrante Smith [41] (BFS) method. These studies show that the model has the Cu-Au type orderings on the fcc lattice for  $k < 0$ . On the other hand, the Cu-Au type binary alloys are studied experimentally by the x-ray diffraction [46] – [50], the nuclear magnetic resonans (NMR) [51], the galvanic cell study [52], the electrical resistivity [53] and the electron diffraction [54, 55]. Some of the experimental studies [47], [49] – [55] and the theoretical studies [40, 41, 45] have indicated that the  $AB$  ordering region separates into two identical regions  $AB$  (type-I) and  $AB$  (type-II). However, one of the the BEG model studies [30] shows the signs about existence of the  $AB$  (type-II) ordering while the spin-1/2 Ising model [37] – [39], [42] – [44] works do not obtain this ordering. Thus, the alternative results are needed to check the differences in results for the Ising model.

In the previous papers, the CCA algorithm and improved versions have been used to study the properties of the critical behaviors of the Ising model hamiltonians [8, 9], [18] – [23], [56] – [70]. The Creutz cellular automaton (CCA) algorithm, which was first introduced by Creutz [56], is a microcanonical algorithm interpolating between the conventional Monte Carlo and the molecular dynamics techniques.

The aim of this study is to investigate the  $A_3B$ ,  $AB$  (type-I),  $AB$  (type-II) and  $AB_3$  type orderings of the Cu-Au type binary alloys on the fcc BEG model using the heating algorithm [8, 9] improved from cellular automaton.

Therefore the fcc BEG model is simulated on a Cellular Automaton (CA) for several sets of parameters  $k$  and  $d$  in the  $-24 \leq d < 0$  and  $-3 \leq k \leq -1.35$  parameter region. For this purpose, the temperature variations of the four sublattice order parameters ( $m_\alpha, q_\alpha$ ), the four sublattice susceptibilities ( $\chi_\alpha$ ), the lattice specific heat ( $C/k$ ) and the lattice Ising energy ( $H_I$ ) were computed on the fcc lattice with linear dimension  $L = 9$  for  $J > 0$ . The finite lattice critical temperatures are estimated from the maxima of the specific heat ( $C/k$ ) and the sublattice susceptibilities ( $\chi_\alpha$ ) to get the phase diagrams. In this study, we have used a heating algorithm improved from the cellular automaton algorithm which successfully produces the critical behavior [8, 9] for the BEG model.

## 2. Results and discussion

The simulations have been performed on the face-centered cubic lattice for linear dimension  $L = 9$  with periodic boundary conditions using heating algorithm (The total number of sites is  $N = 4L^3$ ). This algorithm is realized by increasing of 5% in the kinetic energy ( $H_k$ ) of each site. Therefore, the increasing value per site of  $H_k$  is obtained from the integer part of the  $0.05H_k$ . The computed values of the thermodynamic quantities are averages over the lattice and over the number of time steps (1.000.000) with discard of the first 100.000 time steps during which the cellular automaton develops. The fcc lattice can be built from the four interpenetrating simple cubic (sc) lattices, called sublattices. In this study we used eight order parameters ( $m_\alpha, q_\alpha$ ) to

describe phases for the fcc lattice.

$$m_\alpha = \langle S_i \rangle_\alpha = \frac{1}{N_\alpha} \sum_{i=1}^{N_\alpha} S_{i\alpha} \quad (2)$$

$$q_\alpha = \langle S_i^2 \rangle_\alpha = \frac{1}{N_\alpha} \sum_{i=1}^{N_\alpha} S_{i\alpha}^2 \quad (3)$$

where  $\alpha$  indicate sublattices ( $\alpha = a, b, c, d$ ) (Figure 1).

However we have used the six different phase definitions which were defined according to the values of the sublattice order parameters for  $k \leq -1$  [31]:

Paramagnetic ( $P$ )  $m_a = m_b = m_c = m_d = 0, q_a = q_b = q_c = q_d,$

Ferromagnetic ( $F$ )  $m_a = m_b = m_c = m_d \neq 0, q_a = q_b = q_c = q_d,$

Paramagnetic  $A_3B(P)$   $m_a = m_b = m_c = m_d \neq 0, q_a = q_b = q_c < q_d,$

Ferrimagnetic  $A_3B(f)$   $0 < m_a = m_b = m_c < m_d, q_a = q_b = q_c < q_d,$

Ferrimagnetic  $AB$  (type-I)  $m_a = m_b > m_c = m_d > 0, q_a = q_b > q_c = q_d,$

Ferrimagnetic  $AB$  (type-II)  $0 < m_a = m_b < m_c = m_d, q_a = q_b < q_c = q_d,$

Ferrimagnetic  $AB_3(f)$   $m_a = m_b = m_c > m_d > 0, q_a = q_b = q_c > q_d.$

The ground state diagram of the fcc BEG model is illustrated in Figure 2. It is shown that the ground state phase diagram of the fcc BEG model on the  $(k, d)$  plane has the ferromagnetic ( $F$ ), the staggered quadrupolar ( $SQ$ ) and the quadrupolar ( $Q$ ) ordering regions. Furthermore the staggered quadrupolar ordering region separates into three regions which have the  $A_3B$ ,  $AB$  and  $AB_3$  orderings [31].

### 2.1. The phase diagrams

The critical behavior of the BEG model near the phase boundaries is investigated using CA algorithm on the  $k=-3$  and  $d=-4$  lines. For  $k = -3$ , the

estimated  $(kT_C/zJ, d)$  phase diagram is shown in Figure 3 comparing with the CVM results [31]. As it is seen in Figure 3, the model exhibits  $A_3B(P)$ ,  $A_3B(f)$ ,  $AB(f)$ ,  $AB_3(f)$ ,  $F$  and  $P$  orderings on the  $(kT_C/zJ, d)$  plane for the fcc BEG model at  $k = -3$ . There are some difference between the CA and the CVM results. The CVM introduced that only the  $A_3B(f)$ - $A_3B(P)$  and the  $P-F$  phase transitions are of the second order while the other transitions are of the first order. However our calculations shown that the first order phase transitions occur only at the  $-6 \leq d < 0$  and  $-16 < d \leq -15.5$  parameter regions and  $d = -12$  and  $-20$  parameter values. Furthermore the calculations have demonstrated the  $AB$  (type-II) ordering region in the phase diagram as indicated by the experimental results [47], [49] – [55].

The  $(kT_C/zJ, k)$  phase diagram for  $d = -4$  is presented in Figure 4. As it is seen from Figure 4, there are the  $A_3B(P)$ ,  $AB$  (type-I),  $AB$  (type-II),  $AB_3(f)$ ,  $F$  and  $P$  orderings as seen in the  $(kT_C/zJ, d)$  phase diagram for  $k = -3$ . However, the  $A_3B(f)$  ordering does not appear for  $d = -4$  which occur for  $k = -3$  in the interval  $-8 < d \leq -7.3$ . The simulation results show that the  $F - A_3B(P)$  and the  $P - A_3B(P)$  phase transitions in the  $-3 \leq k \leq -2$  parameter region, the  $F - AB(f)$  phase transition at  $k = -1.8$  value and the  $F - AB_3(f)$  phase transitions in the  $-1.41 < k \leq -1.35$  parameter region are of the first order while the other transitions are of the second order. Therefore, the existence of the phase boundaries between  $A_3B$ ,  $AB$  and  $AB_3$  ground state ordering regions on the  $(k, d)$  plane which is illustrated in Figure 2 are supported by the  $(kT_C/zJ, d)$  and the  $(kT_C/zJ, k)$  phase diagrams for  $k = -3$  (Figure 3) and  $d = -4$  (Figure 4), respectively. In

addition, the successive  $P-F-AB$  (type-II)– $AB$  (type-I) phase transitions occur in the interval  $-2 < k \leq -1.5$ .

## 2.2. The phase transitions on the Cu-Au type orderings

The temperature variations of the sublattice order parameters ( $m_\alpha, q_\alpha$ ), the sublattice susceptibility ( $\chi_a$ ), the lattice Ising energy ( $H_I$ ), and the lattice specific heat ( $C/k$ ) are calculated to determine the types of the phase transitions for  $k = -3$  in the interval  $-24 \leq d < 0$  and for  $d = -4$  in the interval  $-1.41 < k \leq -1.35$ . For producing the phase diagrams, the finite lattice critical temperatures are estimated from the maxima of the specific heat ( $C/k$ ) and the sublattice susceptibilities ( $\chi_\alpha$ ) on the lattice with  $L = 9$ .

The temperature dependences of the quantities are given in Figure 5 for representing the  $P-A_3B(P)$  phase transition at a selected ( $d = -4, k = -3$ ) point on the ( $k, d$ ) plane. At this transition, the sublattice order parameters and the Ising energy are in s-shape nature (Figure 5(a) and 5(c)) while the sublattice susceptibilities and the specific heat show a sharp peak at the transition temperature  $T_{t1}$  (Figure 5(b) and 5(d)). Therefore, the  $P-A_3B(P)$  phase transition is of first order. The model exhibits similar behavior for  $-6.1 < d \leq 0$  parameter region.

In the  $-8 < d \leq -7.3$  parameter region for  $k = -3$ , CA results show that there are successive  $P-F-A_3B(f)-A_3B(P)$  phase transitions. The temperature variations of the sublattice order parameters ( $m_\alpha, q_\alpha$ ), the sublattice susceptibility ( $\chi_a$ ), the lattice Ising energy ( $H_I$ ), and the lattice specific heat ( $C/k$ ) are illustrated in Figure 6 for selected  $d = -7.7$  parameter value. As it is seen in Figure 6, the sublattice order parameters and the lattice Ising

energy exhibit continuity (Figure 6(a) and 6(c)). However, the sublattice susceptibility and the lattice specific heat have three characteristic peaks at the critical temperatures  $T_{C1}$ ,  $T_{C2}$  and  $T_{C3}$  (Figure 6(b) and 6(d)). Therefore, the successive phase transitions are of the second order. On the other hand, the  $F-A_3B(f)$  phase transition is of the first order according to the CVM [31] results (Figure 3).

In the interval  $-15.5 < d < -8.3$  for  $k = -3$ , CA simulations show that the model exhibit the successive  $P - F - AB$  (type-II)– $AB$  (type-I) phase transitions except  $d = -12$  parameter value. For  $d = -12$ , there is the successive  $P - F - AB$  (type-I) phase transitions. In Figure 7, temperature variations of the sublattice order parameters ( $m_\alpha, q_\alpha$ ), the sublattice susceptibility ( $\chi_a$ ), the lattice Ising energy ( $H_I$ ), and the lattice specific heat ( $C/k$ ) are illustrated for ( $d = -12, k = -3$ ) value. At the  $F - AB$  (type-I) phase transition, the sublattice order parameters are in s-shape nature at the transition temperature  $T_{t1}$ (Figure 7(a)). The inset in the Figure 7(c) shows that the lattice Ising energy are in s-shape nature at the same transition temperature. However, the sublattice order parameters and the lattice specific heat appear continuously for the  $P - F$  phase transition (Figure 7(a) and 7(c)). At the same time, the sublattice susceptibility and the lattice specific heat have a sharp peak at  $T_{t1}$  and a characteristic peak at  $T_{C1}$  for these transitions (Figure 7(b) and 7(d)). This results show that the  $F - AB$ (type-I) and the  $P - F$  phase transitions are of the first and the second order, respectively.

In the intervals  $-15.5 < d < -12$  and  $-12 < d < -8.3$ , the model has the  $AB$  (type-II) ordering. The  $AB$  (type-II) ordering is determined from



the behavior of the sublattice order parameters  $(m_\alpha, q_\alpha)$ . The temperature dependences of the quantities show that the model exhibit the successive  $P - F - AB$  (type-II)– $AB$  (type-I) phase transitions in these intervals (Figure 8). It can be seen from Figure 8, for  $d = -13$ , the sublattice order parameters and the lattice Ising energy show continuity at the  $P - F$  and the  $AB$  (type-II)– $AB$  (type-I) phase transitions (Figure 8(a) and 8(c)) while the sublattice susceptibilities and the lattice specific heat have two characteristic peaks (Figure 8(b) and 8(b)) at  $T_{C1}$  and  $T_{C3}$ . However, the sublattice susceptibilities  $(\chi_\alpha)$  and the lattice specific heat  $(C/k)$  do not show any peak for the  $F - AB$  (type-II) phase transition. The critical temperature  $T_{C2}$  of this transition is estimated from the sublattice order parameters (Figure 8(a)). As it is seen in Figure 8(a) the sublattice order parameters become equal at a critical temperature  $(T_{C2})$ .

The model exhibit the reentrant behavior at phase boundary between the  $AB$  (type-I) and the  $AB_3(f)$  regions. The temperature variations of the quantities for  $d = -15.8$  parameter value are shown in Figure 9. There are the successive  $P - F - AB$  (type-I)– $F - AB$  (type-I) phase transitions. For the first order  $F - AB$  (type-I) phase transition, the sublattice order parameters and the lattice Ising energy are in s-shape nature (Figure 9(a) and 9(c)) while the sublattice susceptibility and the lattice specific heat show a sharp peak at  $T_{t1}$ (Figure 9(b) and 9(d)). However, the  $P - F - AB$  (type-I)– $F$  phase transitions are of the second order.

In the interval  $-24 < d < -16$ , the model shows the successive  $P - F - AB_3(f)$  phase transitions for  $k = -3$ . At a selected  $(d = -20, k = -3)$  value,

the temperature variation of the quantities are illustrated in Figure 10. At the  $F - AB_3(f)$  phase transition, the sublattice order parameters and the lattice Ising energy are in s-shape nature while the sublattice susceptibilities and the lattice specific heat have a sharp peak at  $T_{t1}$ . However, the sublattice susceptibilities and the lattice specific heat have a characteristic peak at  $T_{C1}$  for the  $P - F$  phase transition. Therefore, the  $F - AB_3(f)$  and the  $P - F$  phase transitions are of the first and the second order, respectively.

### 3. Conclusion

The spin-1 Ising BEG model has been simulated using the heating algorithm on the cellular automaton for the face-centered cubic lattice. The simulations show that the BEG model have the Cu-Au type stoichiometric  $A_3B$ ,  $AB$  and  $AB_3$  orderings in the staggered quadrupolar region for  $k < -1$ . Furthermore, the  $A_3B$ ,  $AB$  and  $AB_3$  ordering regions exhibit the successive phase ransitions. The phase diagram on the  $(kT_C/zJ, d)$  plane is compared with the Cluster Variation Method [31] (CVM) results for  $k = -3$ . Moreover, the phase diagram on the  $(kT_C/zJ, k)$  plane is obtained for  $d = -4$ . It is seen that the cellular automaton (CA) results support the phase boundaries on the  $(k, d)$  plane and  $(kT_C/zJ, d)$  phase diagrams which obtained by the CVM for  $k = -3$ . However, for some parameter values the phase transition types have been obtained different from the CVM [31] results on the  $(kT_C/zJ, d)$  plane. The CVM [31] and our results show that the fcc BEG model has the Cu-Au type orderings in the staggered quadrupolar ordering region ( $k < -1$ ). In addition, we obtain that the fcc BEG model has the  $AB$  (type-II) ordering and exhibit the  $AB$  (type-II)– $AB$  (type-I) phase

transition as indicated by the experimental results [47], [49] – [55].

### Acknowledgement

This work is supported by a grant from Gazi University (BAP:05/2003-07).

- [1] Blume M, Emery V J and Griffiths R B, 1971 *Phys. Rev. A* **4**, 1071
- [2] Lajzerowicz J and Siverdière J, 1975 *Phys. Rev. A* **11**, 2079
- [3] Lajzerowicz J and Siverdière J, 1975 *Phys. Rev..A* **11**, 2090; **11**, 2101
- [4] Schick M and Shih W H, 1986 *Phys.Rev. B* **34**, 1797
- [5] Newman K E and Dow J D, 1983 *Phys. Rev. B* **27**, 7495
- [6] Kessler M, Dieterich W and Majhofer A, 2003 *Phys. Rev. B* **67**, 134201
- [7] Hoston W and Berker A N, 1991 *Phys. Rev. Lett.* **67**, 1027
- [8] Seferoğlu N and Kutlu B, 2007 *Physica A* **374**, 165
- [9] Özkan A, Kutlu B, *Int.J.of Mod.Phys C*, (accepted to publish)
- [10] Saul D M, Wortis M and Stauffer D, 1974 *Phys. Rev. B* **9** 4964
- [11] Koza Z, Jasuukiewicz C, Pekalski A, 1990 *Physica A* **164** 191
- [12] Berker A N, Wortis M, 1974 *Phys. Rev. B* **14** 4946
- [13] Takahashi K, Tanaka M, 1979 *J. Phys. Soc. Japan* **46** 1428
- [14] Albayrak E, Keskin M, 2000 *J. Magn. Magn. Mater.* **203** 201
- [15] Keskin M, Ekiz C, Yalçın O, 1999 *Physica A* **267** 392
- [16] Jain A K and Landau D P, 1980 *Phys. Rev. B* **22** 445
- [17] Costeniuc M, Ellis R S, Otto P T, 2007 *J. of Stat. Phys.* **127**, 3
- [18] Solak A and Kutlu B, 2004 *Int. J. Mod. Phys. C* **15** 1425
- [19] Kutlu B, 2001 *Int. J. Mod. Phys. C* **14** 1401

- [20] Kutlu B, 2003 *Int. J. Mod. Phys. C* **14** 1305
- [21] Kutlu B, Özkan A, Seferoğlu N, Solak A and Binal B, 2005 *Int. J. Mod. Phys.C* **16** 933
- [22] Özkan A, Seferoğlu N and Kutlu B, 2006 *Physica A* **362** 327
- [23] Seferoğlu N and Özkan A and Kutlu B, 2006 *Chin. Phys. Lett.* **23**, 2526
- [24] Netz R R, Berker A N, 1993 *Phys. Rev.B* **47** 15019
- [25] Hoston W and Berker A N, 1991 *J. App. Phys.* **70** 6101
- [26] Wang Y L, Lee F, Kimel J D, 1987 *Phys. Rev. B* **36** 8945
- [27] Wang Y L, Wentworth C, 1987 *J. Appl. Phys.* **61** 4411
- [28] Tanaka M, Kawabe T, 1985 *J. Phys. Soc. Japan* **54** 2194
- [29] Kasono K, Ono I, 1992 *Z.Phys. B: Condens. Matter* **88** 205
- [30] Kundrotas P J, Lapinskas S and Rosengren A, 1997 *Phys. Rev. B* **56**, 6486
- [31] Lapinskas S and Rosengren A, 1993 *Phys. Rev. B* **49**, 15190
- [32] Ekiz C and Keskin M, 2002 *Phys. Rev. B* **66**, 054105
- [33] Keskin M, Erdiñç A, 2004 *J. Magn. Magn. Mater.* **283**, 392
- [34] Tucker J W, Balcerzak T, Gzik M, Sukiennicks A, 1998 *J. Magn. Magn. Mater.* **187** 381
- [35] Netz R R, 1992 *Europhys. Lett.* **17**, 373
- [36] Baran O R, Levitskii R R, 2002 *Phys. Rev.B* **65**, 172407
- [37] Phani M K, Lebowitz J L, Kalos M H, Tsai C C, 1979 *Phys. Rev. Lett.* **42**, 577
- [38] Binder K, 1980 *Phys. Rev. Lett.* **45**, 811

- [39] Styer D F, Phani M K, Lebowitz J L, 1986 *Phys. Rev.B* **34**, 3361
- [40] Xi Z, Chakraborty B, Jacobsen K W, Norskov J K, 1992 *J.Phys:Cond. Matt.* **4**, 7191
- [41] Bozzolo G, Good B, Ferrante J, 1996 *NASA Technical Memorandum* 107168
- [42] Wei S H, Mbaye A A, Ferreira L G, Zunger A, 1987 *Phys. Rev. B* **36**, 4163
- [43] Sanchez J M, Lin C H, 1984 *Phys. Rev. B* **30**, 1448
- [44] Beath A D, Ryan D H, 2005 *Physical Rev. B* **72**, 014455
- [45] Chakraborty B, Xi Z, 1992 *Phys. Rev. Lett.* **68**, 2039
- [46] Barbier L, Goapper S, Salanon B, Caudron R, Loiseau A, Alvarez J, Ferrer S, Torrelles X, 1997 *Phys. Rev. Lett.* **78**, 3003
- [47] Jordan R G, Jiang Y, Hoyland M A, Begley A M, 1991 *Physical Rev.B* **43**, 12173
- [48] Guhr I L, Riedlinger B, Maret M, Mazur U, Barth A, Treubel F, Albrecht M, Schatz G, 2005 *J. of Applied Physics* **98**, 063520
- [49] Bain E C, 1923 *Chem. Met. Eng.* **28**, 21
- [50] Pianelli A, Faivre R, 1957 *Compt. Rend.* **245**, 1537
- [51] Shinohara T, Saitoh S, Wagatsuma F, Yamaguchi S, 1999 *Philosophical Magazine A* **79**, 437
- [52] Oriani R A, 1954 *Acta metall.* **2**, 608
- [53] Rhines F N, Bond W E, Rummel R A, 1955 *Trans. Amer. Soc. Met.* **47**, 578
- [54] Sato H, Toth R S, 1961 *Phys. Rev.* **124**, 1833

- [55] Sato K, Watanabe D, Ogawa S, 1962 *J. Pyhs. Soc. Jpn* **17**, 1647
- [56] Creutz M, 1983 *Phys. Rev. Lett.* **50**, 1411
- [57] Kutlu B, Aktekin N, 1994 *J. Stat.Phys.* **75**, 757
- [58] Kutlu B, Aktekin N, 1995 *Physica A* **215**, 370
- [59] Kutlu B, 1997 *Physica A* **234**, 807
- [60] Kutlu B, 1997 *Physica A* **243**, 199
- [61] Aktekin N, *Annual Reviews of computational physics* **VII**, ed. D.Stauffer (World Scientific, Singapore, 2000) p. 1.
- [62] Dress C, *J.of physics A* **28**, 7051(1995).
- [63] Saito K, Takesue S and Miyashita S, 1999 *Phys.Rev.E* **59**, 2783
- [64] Gwizdella T M , 2004 *Czechoslovak J. of Phys.* **54**, 679
- [65] Merdan Z, Bayırlı M, 2005 *Applied Mathematics and Computation* **167**, 212
- [66] Gwizdella T M, *Mod. 2005 Phys. Lett. B* **19**, 169
- [67] Merdan Z, Atille D, 2007 *Physica A* **376**, 327
- [68] Aktekin N, Erkoç S, 2001 *Physica A* **290**, 123
- [69] Aktekin N, Erkoç S, 2000 *Physica A* **284**, 206
- [70] Merdan Z, Erdem R, 2004 *Phys. Lett. A* **330**, 403

### Figure Captions

Figure 1. The four sublattices for an fcc lattice. The circle, the square, the diamond and the triangle indicate the  $m_a$ ,  $m_b$ ,  $m_c$  and  $m_d$  sublattices, respectively.

Figure 2. The ground state phase diagram  $(k, d)$  of the BEG model on the fcc lattice.

Figure 3. The phase diagram in the  $(kT_C/zJ, d)$  plane for  $k = -3$ . Solid and dashed lines indicate the second and the first order phase transitions for CVM<sup>[29]</sup> results. Full and open circles indicate the second and the first order phase transitions and the thin line is guide to eye for CA results.

Figure 4. The phase diagram in the  $(kT_C/zJ, k)$  plane for  $d = -4$ . Full and open circles indicate the second and the first order phase transitions for CA results

Figure 5 For  $d = -4$ , the temperature dependence of (a) sublattice order parameters  $(m_\alpha, q_\alpha)$ , (b) the sublattice susceptibility  $(\chi_a)$ , (c) the lattice Ising energy  $(H_I)$ , and (d) the lattice specific heat  $(C/k)$  at  $k = -3$ .

Figure 6. For  $d = -7.7$ , the temperature dependence of (a) sublattice order parameters  $(m_\alpha, q_\alpha)$ , (b) the sublattice susceptibility  $(\chi_a)$ , (c) the lattice Ising energy  $(H_I)$ , and (d) the lattice specific heat  $(C/k)$  at  $k = -3$ .

Figure 7. For  $d = -12$ , the temperature dependence of (a) sublattice order parameters  $(m_\alpha, q_\alpha)$ , (b) the sublattice susceptibility  $(\chi_a)$ , (c) the lattice Ising energy  $(H_I)$ , and (d) the lattice specific heat  $(C/k)$  at  $k = -3$ .

Figure 8. For  $d = -13$ , the temperature dependence of (a) sublattice order parameters  $(m_\alpha, q_\alpha)$ , (b) the sublattice susceptibility  $(\chi_a)$ , (c) the lattice Ising energy  $(H_I)$ , and (d) the lattice specific heat  $(C/k)$  at  $k = -3$ .

Figure 9. For  $d = -15.8$ , the temperature dependence of (a) sublattice order parameters  $(m_\alpha, q_\alpha)$ , (b) the sublattice susceptibility  $(\chi_a)$ , (c) the lattice Ising energy  $(H_I)$ , and (d) the lattice specific heat  $(C/k)$  at  $k = -3$ .

Figure 10. For  $d = -20$ , the temperature dependence of (a) sublattice order parameters  $(m_\alpha, q_\alpha)$ , (b) the sublattice susceptibility  $(\chi_a)$ , (c) the lattice

Ising energy ( $H_I$ ), and (d) the lattice specific heat ( $C/k$ ) at  $k = -3$ .



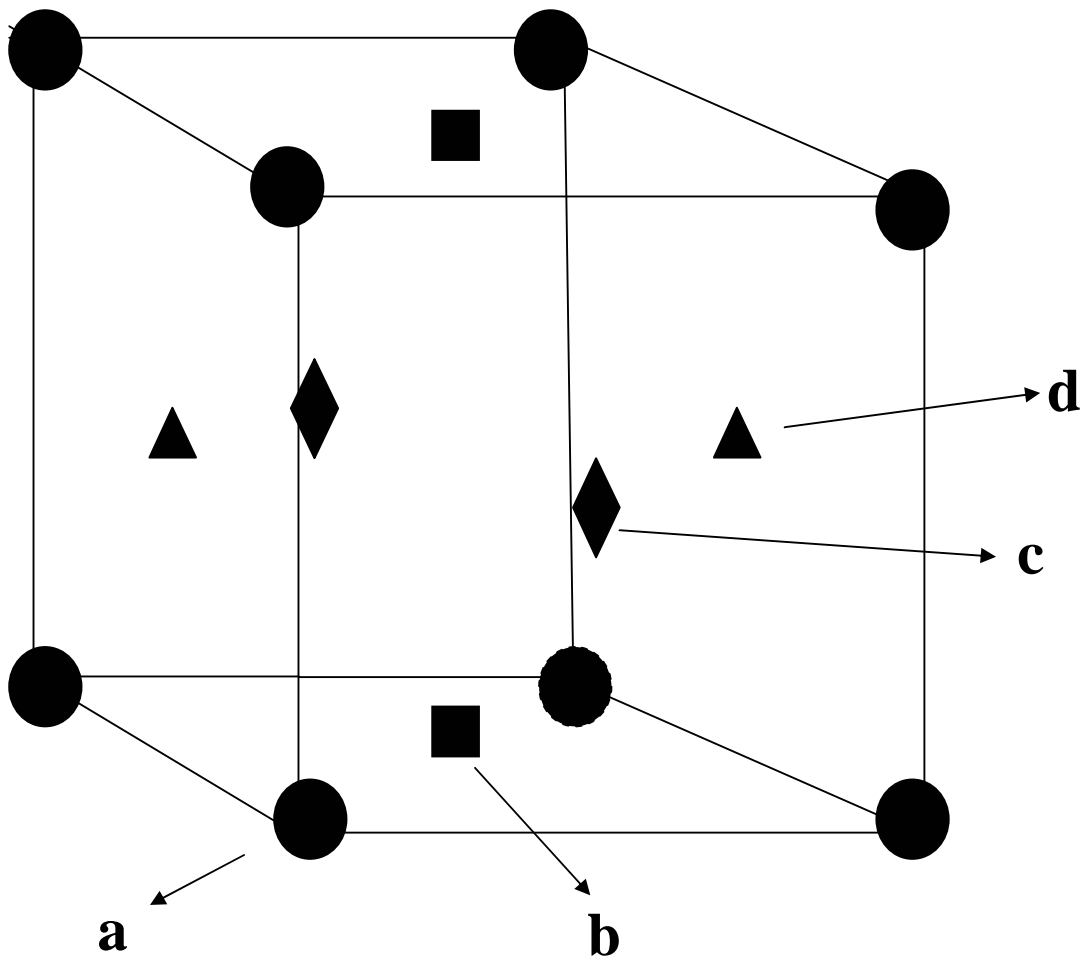


Figure 1

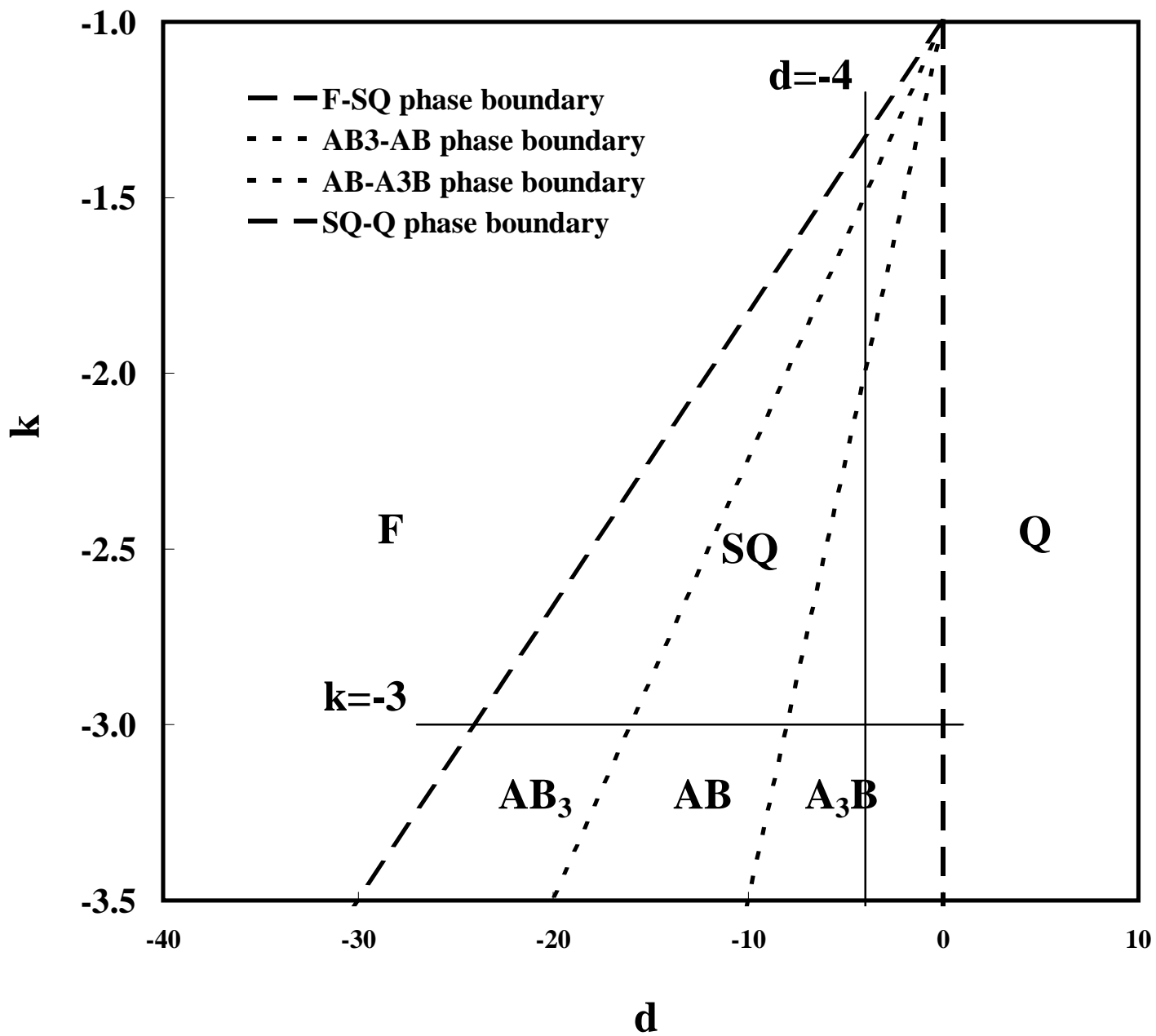


Figure 2

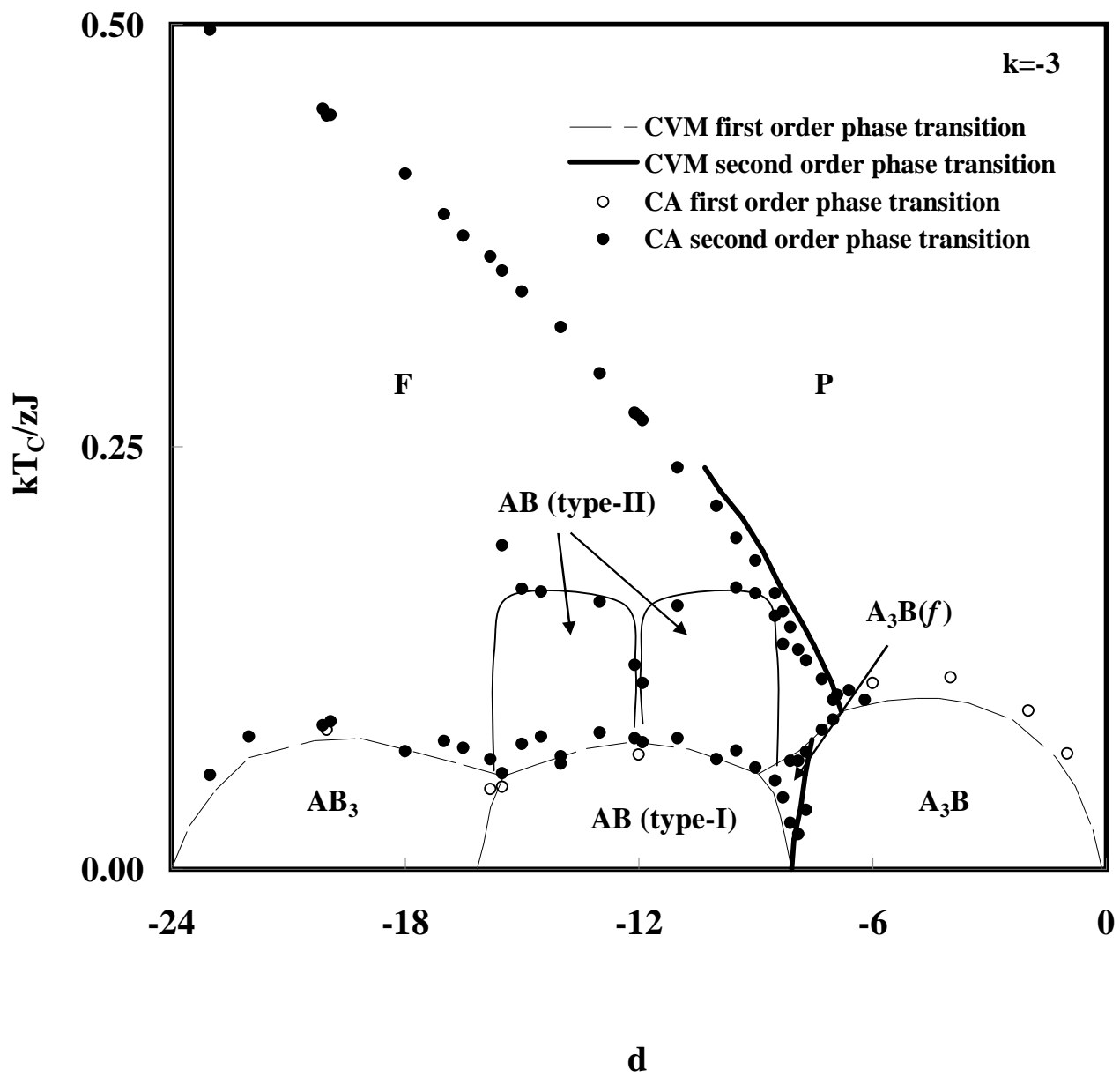


Figure 3

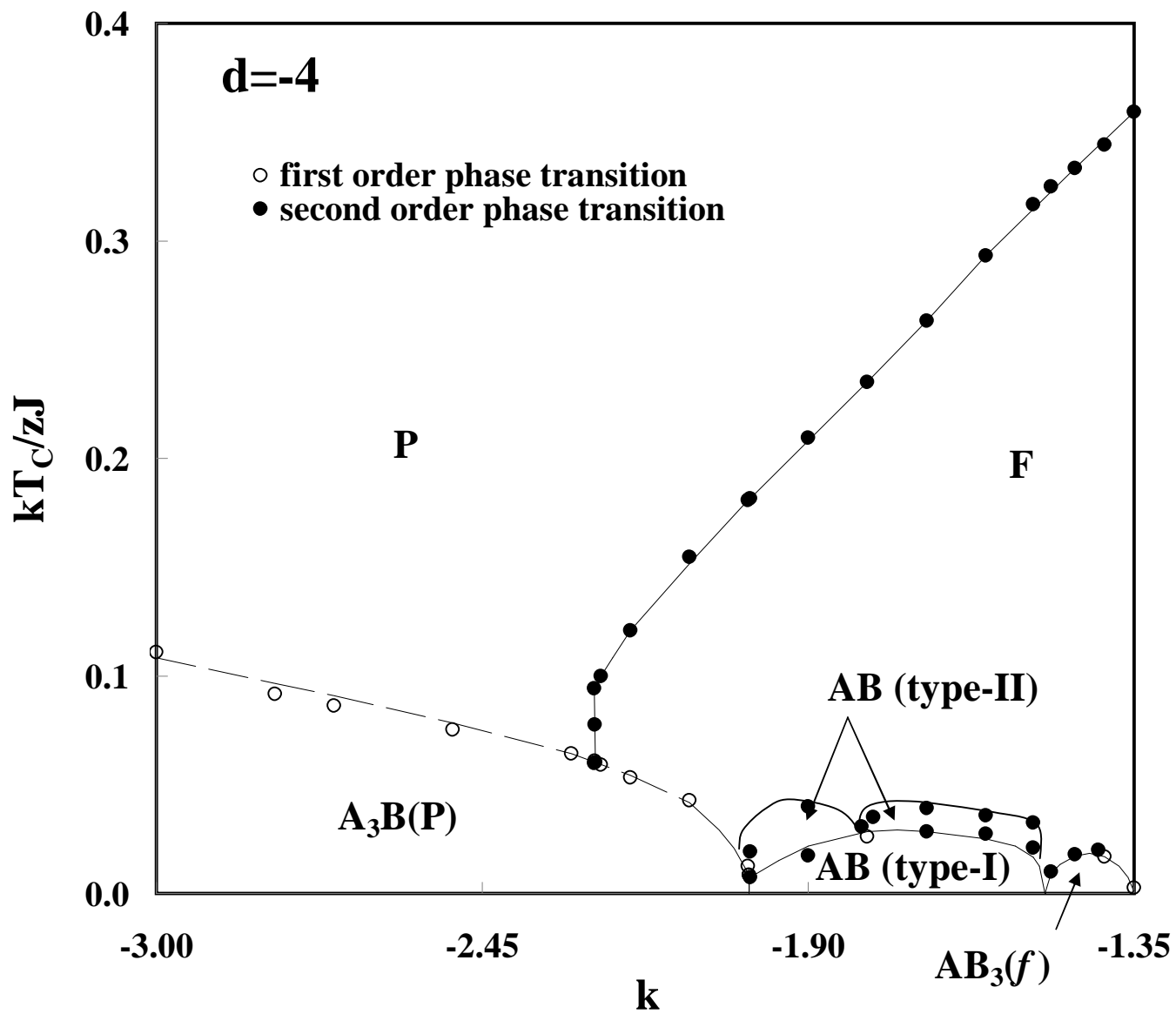


Figure 4

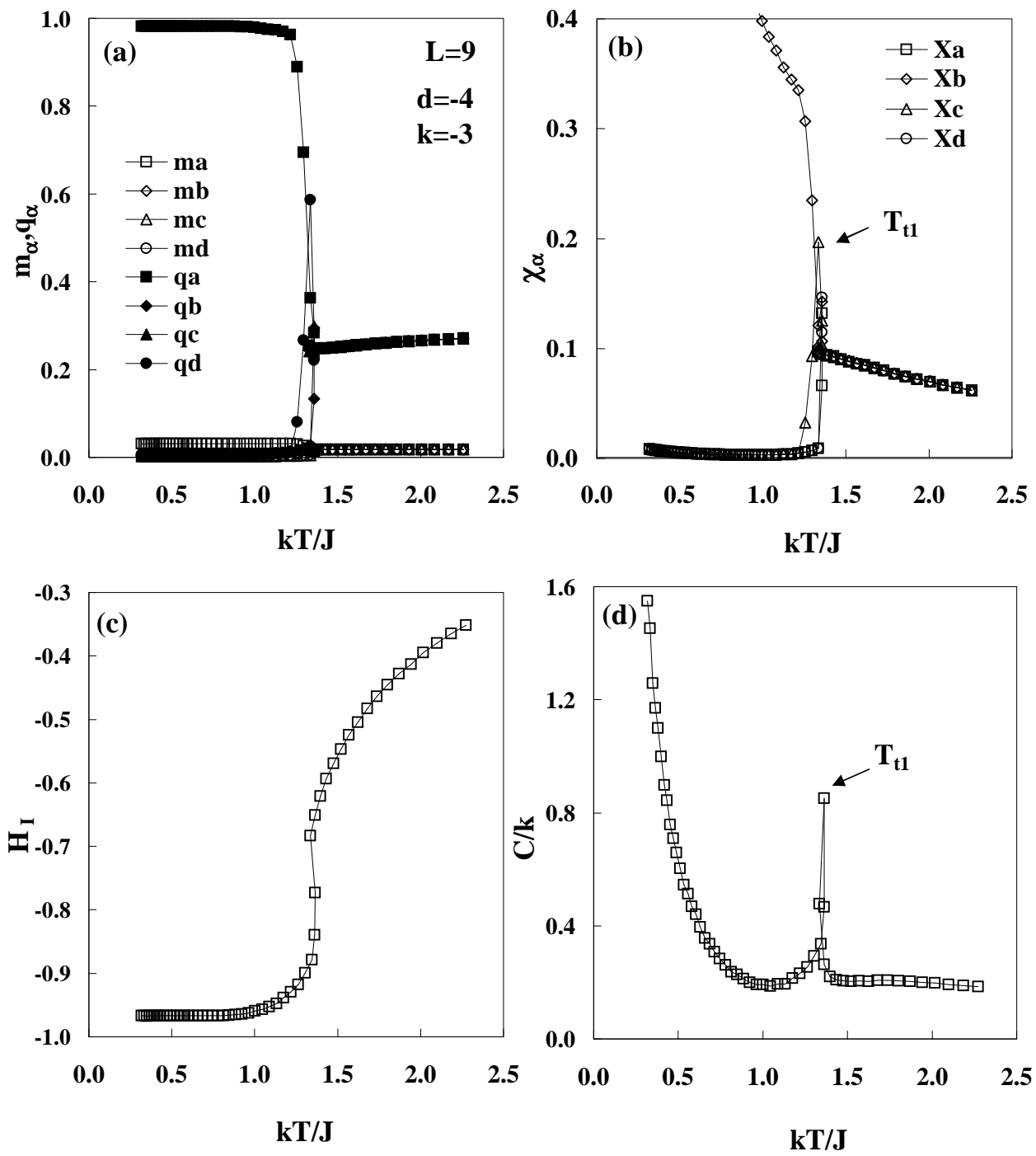


Figure 5

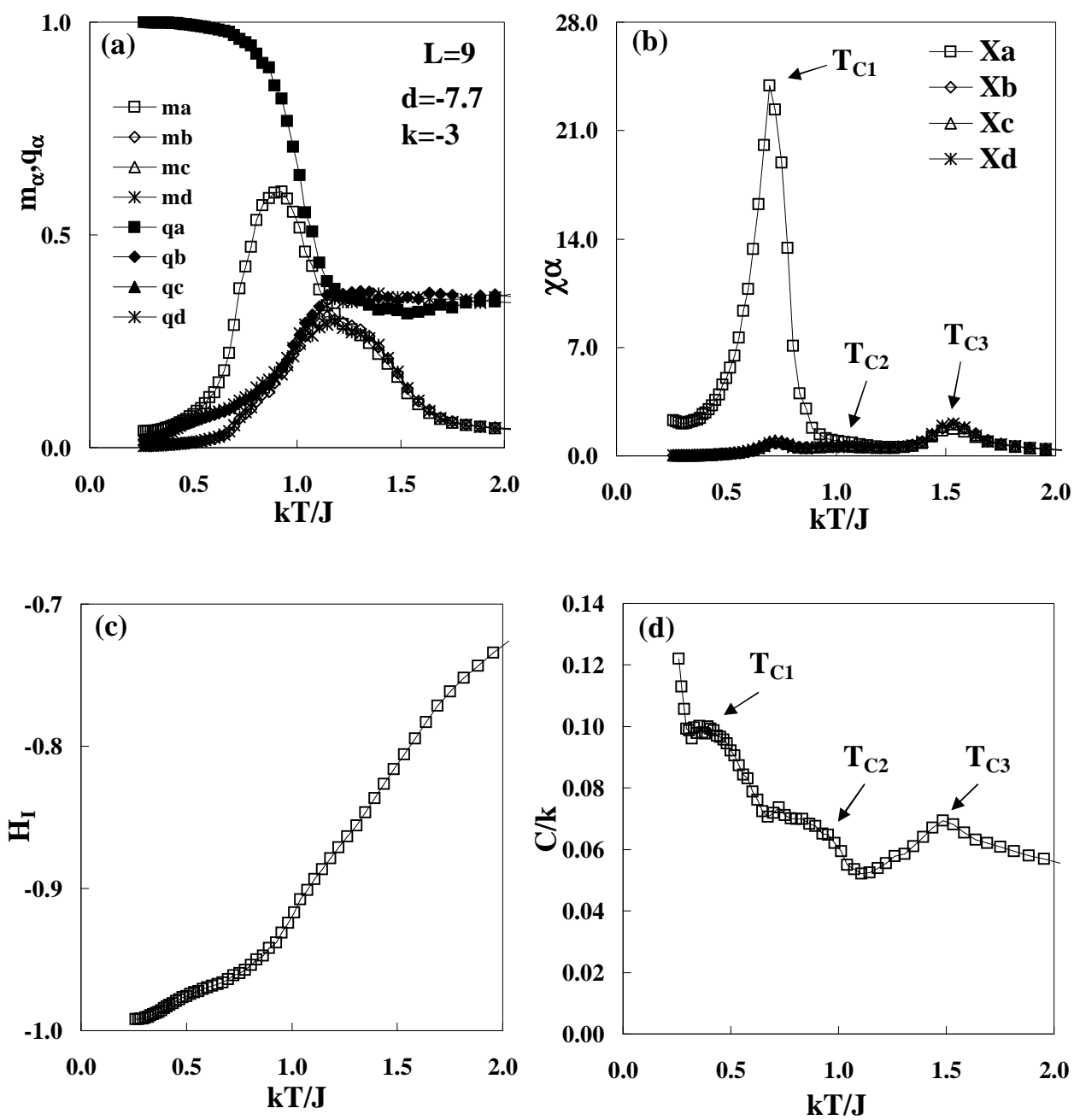


Figure 6

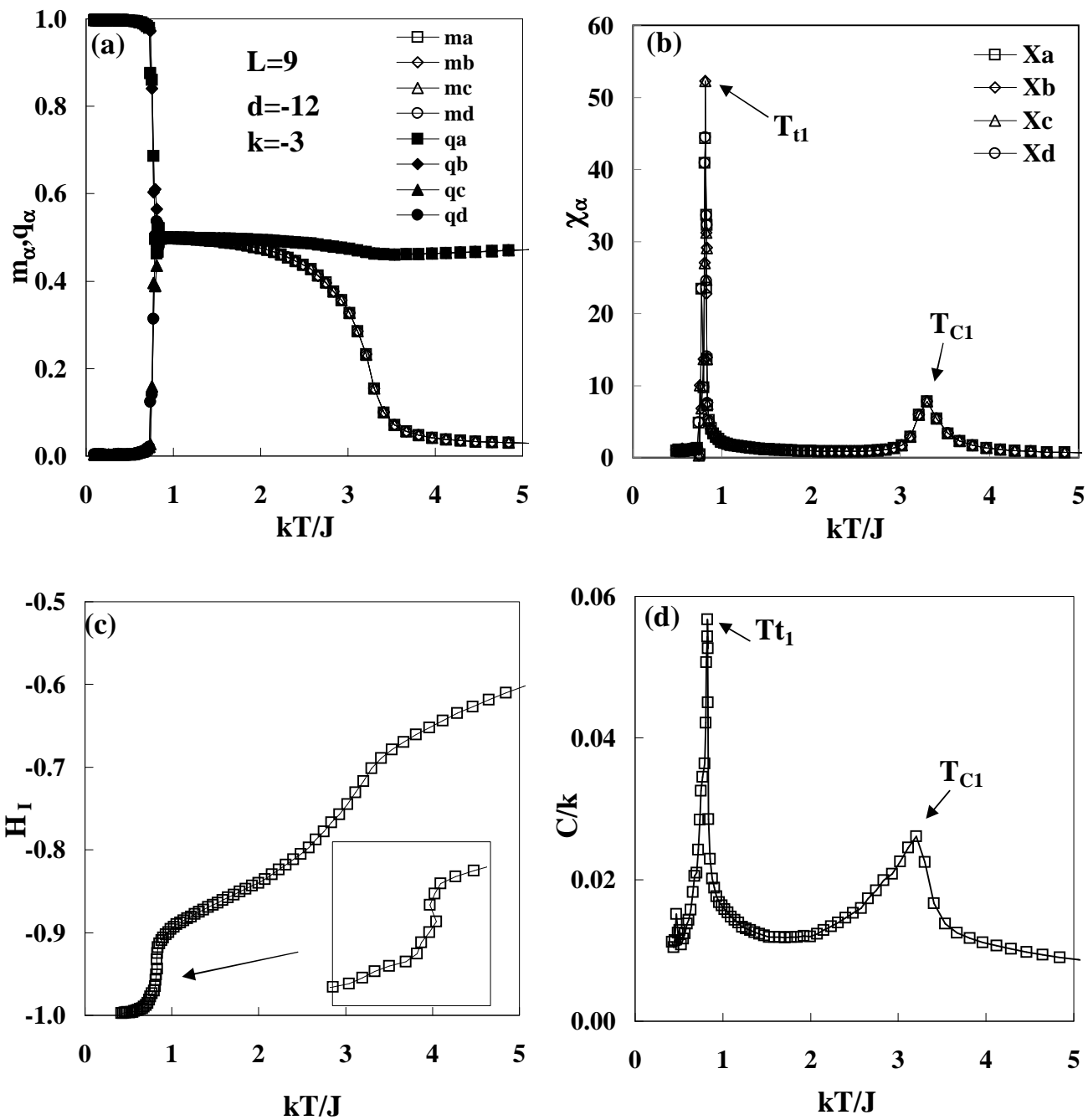


Figure 7

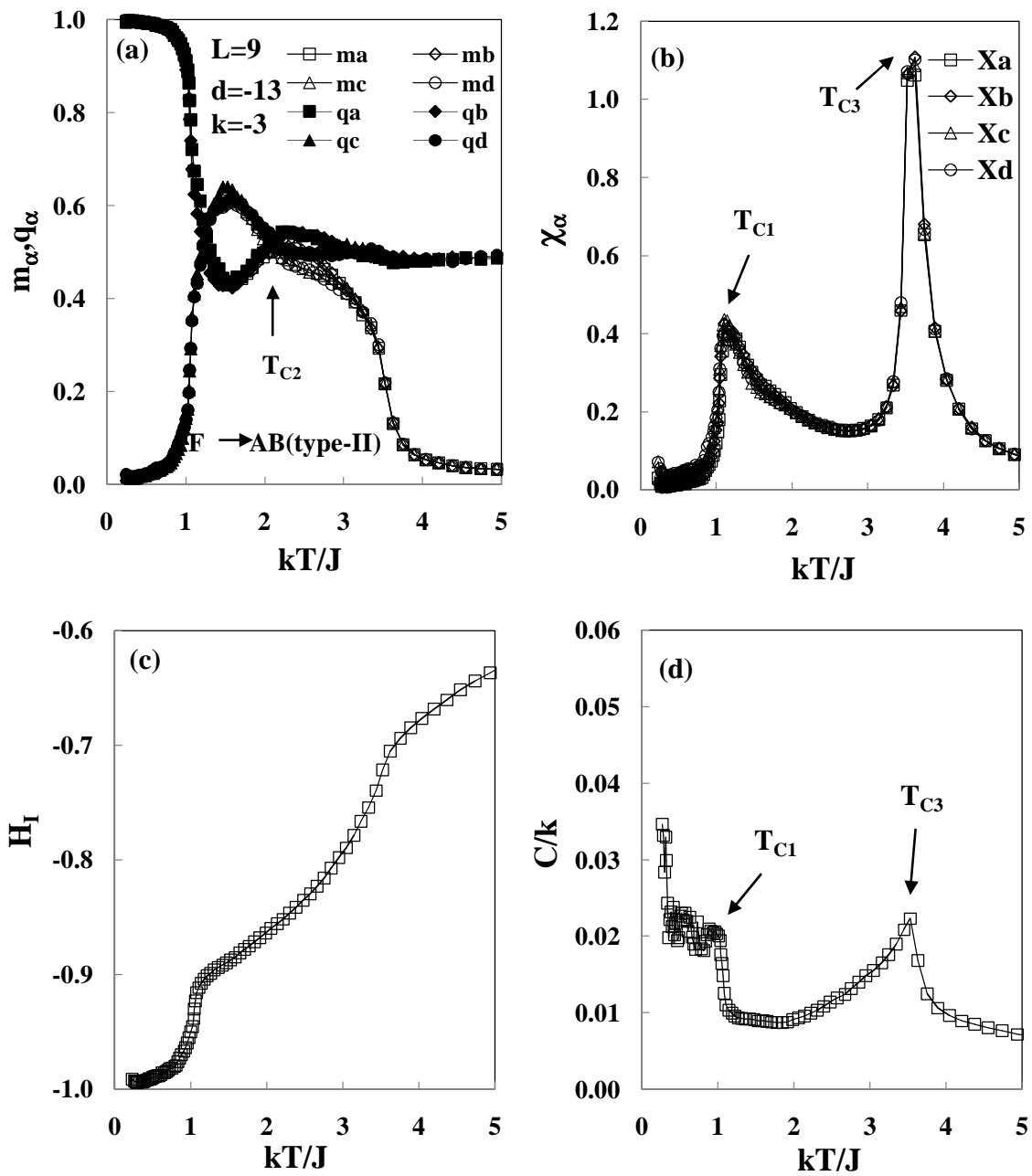


Figure 8



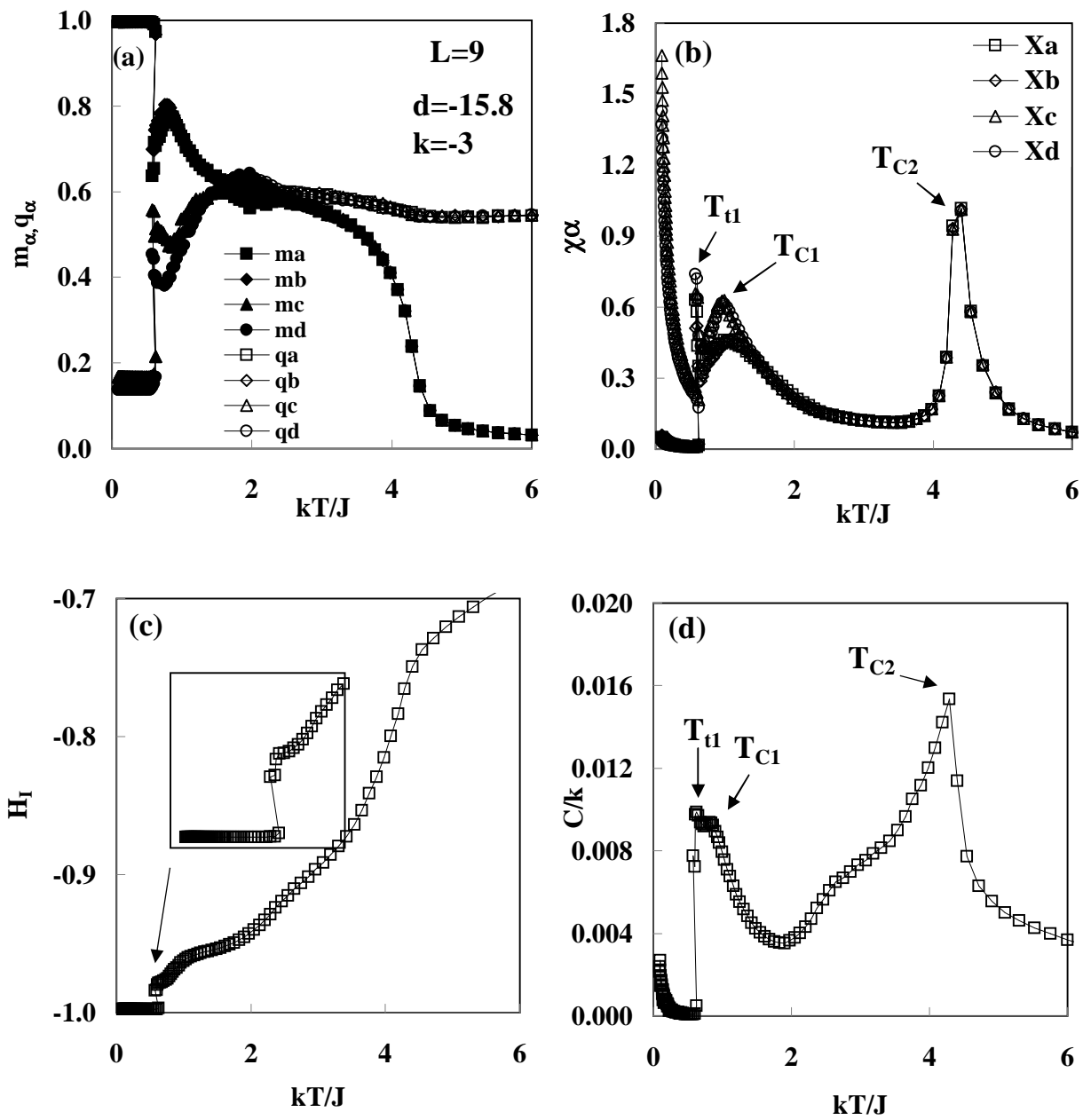


Figure 9

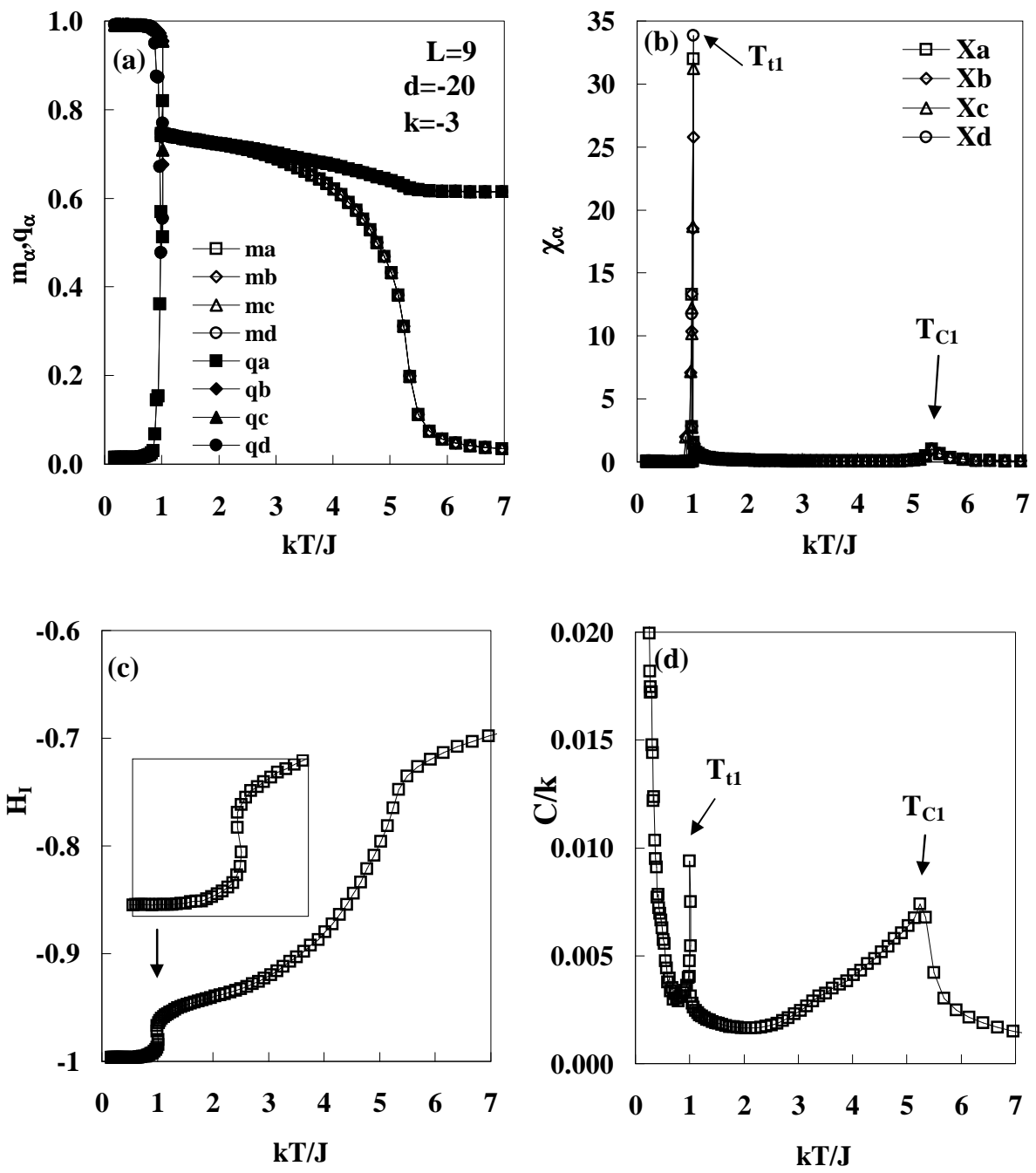


Figure 10